Electrochimica Acta 165 (2015) 348–355

Contents lists available at ScienceDirect

Electrochimica Acta

journal homepage: www.elsevier.com/locate/electacta

Inhibition of Direct Electrolytic Ammonia Oxidation Due to a Change in Local pH

Hanspeter Zöllig, Eberhard Morgenroth, Kai M. Udert *

Eawag, Swiss Federal Institute of Aquatic Science and Technology, Überlandstrasse 133, 8600 Dübendorf, Switzerland

ARTICLE INFO

Article history:
Received 31 January 2015
Received in revised form 17 February 2015
Accepted 18 February 2015
Available online 9 March 2015

Keywords:
Iridium dioxide
low alkalinity
water treatment
Nernstian diffusion layer
acid-base equilibrium

ABSTRACT

Electrochemical ammonia oxidation has gained a lot of attention recently as an efficient method for ammonia removal from wastewater, for the use in ammonia-based fuel cells and the production of high purity hydrogen. Thermally decomposed iridium oxide films (TDIROF) have been shown to be catalytically active for direct ammonia oxidation in aqueous solutions if NH_3 is present. However, the process was reported to be rapidly inhibited on TDIROF. Herein, we show that this fast inhibition of direct ammonia oxidation does not result from surface poisoning by adsorbed elemental nitrogen (N_{ads}). Instead, we propose that direct ammonia oxidation and oxygen evolution can lead to a drop of the local pH at the electrode resulting in a low availability of the actual reactant, NH_3. The hypothesis was tested with cyclic voltammetry (CV) experiments on stagnant and rotating disk electrodes (RDE). The CV experiments on the stagnant electrode revealed that the decrease of the ammonia oxidation peaks was considerably reduced by introducing an idle phase at open circuit potential between subsequent scans. Furthermore, the polarization of the TDIROF electrode into the hydrogen evolution region (HER) resulted in increased ammonia oxidation peaks in the following anodic scans which can be explained with an increased local pH after the consumption of protons in the HER. On the RDE, the ammonia oxidation peaks did not decrease in immediately consecutive scans. These findings would not be expected if surface poisoning was responsible for the fast inhibition but they are in good agreement with the proposed mechanism of pH induced limitation by the reactant, NH_3. The plausibility of the mechanism was also supported by our numerical simulations of the processes in the Nernstian diffusion layer. The knowledge about this inhibition mechanism of direct ammonia oxidation is especially important for the design of electrochemical cells for wastewater treatment. The mechanism is not only valid for TDIROF but also for other electrodes because it is independent of the electrode material.

1. Introduction

Direct ammonia oxidation at catalytically active surfaces can be used for the electrolytic removal of ammonia from wastewater [1,2]. Additionally, the process was suggested for the use in fuel cells where ammonia acts as a substitute for hydrogen [3] and for the production of high purity hydrogen in ammonia electrolyzers [4]. In contrast to indirect oxidation with active chlorine species, which is mostly employed for wastewater treatment, direct ammonia oxidation does not produce chlorinated by-products such as chlorate, perchlorate or organic chlorinated substances. Furthermore, direct oxidation usually proceeds at lower anode potentials than chlorine formation. Consequently, a high current efficiency and a lower specific energy demand can be achieved making direct ammonia oxidation attractive for wastewater treatment.

Direct ammonia oxidation was shown to be technically feasible on isostatically pressed fine grain graphite without concomitant chlorine formation [5]. However, the ammonia removal rate was low in real stored urine ($2.9 \pm 0.3\,gN{\cdot}m^{-2}{\cdot}d^{-1}$) and mineralization of the graphite electrode occurred as a side reaction. Although the mineralization was slow, the graphite electrode has to be considered a consumable. Corrosion problems were also reported with $Ni/Ni(OH)_2$ anodes [6]. In order to reduce maintenance and material consumption, it would be desirable to find more stable electrode materials that are suitable for direct ammonia oxidation.

The catalytic activity for direct ammonia oxidation was demonstrated for thermally decomposed iridium oxide films (TDIROF, [7]) or boron-doped diamond electrodes (BDD, [8]). Both electrodes are stable when they are used as anodes. TDIROF electrodes further have the advantage that they are easy to fabricate and that they have a comparatively low overpotential for

* Corresponding author. Tel.: +41 58 765 5360; fax: +41 58 765 5802.
E-mail address: kai.udert@eawag.ch (K.M. Udert).

http://dx.doi.org/10.1016/j.electacta.2015.02.162

direct ammonia oxidation (Table 1). The low overpotential eventually leads to a high selectivity towards direct ammonia oxidation and to low specific energy requirements. However, the costs for the precious metal iridium are a drawback of this electrode.

Kapałka *et al.* [7] found that ammonia oxidation peaks of consecutive cyclic voltammograms decreased dramatically on TDIROF if the lower return potential was above the hydrogen evolution region (HER). The authors interpreted these results as an electrode deactivation through surface poisoning by adsorbed intermediate nitrogen species ($NH_{2,ads}$, NH_{ads}, N_{ads}) formed during the direct ammonia oxidation process initially proposed by Gerischer and Mauerer [9] for platinum (Pt, Eqs. (1)–(5)).

$$NH_3(aq) \rightleftharpoons NH_{3,ads} \quad (1)$$

$$NH_{3,ads} \rightleftharpoons NH_{2,ads} + H^+ + e^- \quad (2)$$

$$NH_{2,ads} \rightleftharpoons NH_{ads} + H^+ + e^- \quad (3)$$

$$NH_{x,ads} + NH_{y,ads} \rightleftharpoons N_2 + (x+y)H^+ + (x+y)e^- \quad (4)$$

$$NH_{ads} \rightleftharpoons NH_{ads} + H^+ + e^- \quad (5)$$

where x, y = 1 or 2.

This interpretation is often used to explain the decreasing activity of electrodes during direct ammonia oxidation in aqueous media [10]. It is mainly based on the findings of de Vooys *et al.* [11] who identified N_{ads} as an electrode poison on transition metal electrodes (such as Ru, Rh, Pd) and who generalized the mechanism of direct ammonia oxidation (Eqs. (1)–(5)) to transition metal electrodes.

However, deactivation of the electrode by surface poisoning might not be the only process leading to lower ammonia oxidation peaks in cyclic voltammetry (CV). In fact, it has been demonstrated for TDIROF [7] and other electrode materials [5,6,8] that direct ammonia oxidation is highly pH sensitive because the actual reactant is NH_3 while NH_4^+ cannot be oxidized directly. Apparently, direct ammonia oxidation itself (Eqs. (2)–(4)), but also many other anodic processes such as oxygen evolution (Eq. (6)), release a large number of protons.

$$2H_2O \rightarrow O_2 + 4H^+ + 4e^- \quad (6)$$

This can lead to a strong pH drop in the Nernstian diffusion layer if the electrolyte is not buffered. The consequence is a shift in the local ammonia speciation according to the acid-base equilibrium, resulting in a low availability of reactive NH_3.

Table 1
Comparison of onset potentials and peak potentials for direct ammonia oxidation on thermally decomposed iridium oxide films (TDIROF), isostatically pressed fine grain graphite and boron-doped diamond (BDD) at pH = 9.

Electrode Material	On-set potential [V vs. SHE]	Peak potential [V vs. SHE]
TDIROF [7]	0.9	1.1
Graphite [5]	1.0	1.4
$Ni/Ni(OH)_2$ [6]	1.1	1.3
BDD [8]	1.6	2.2

The hypothesis of this study is that decreasing ammonia oxidation peaks on TDIROF in subsequent scans could be due to a drop of the local pH in the Nernstian diffusion layer caused by acidic anodic reactions. To test this hypothesis, we evaluated the ammonia oxidation peaks of CV experiments with varying lower return potentials in stagnant electrolytes. Furthermore, we employed a rotating disc electrode (RDE) to control the thickness of the Nerstian diffusion layer under well-defined hydraulic conditions. These experiments were complemented with numerical simulations of the ammonia concentration profiles in the Nernstian diffusion layer to show that the proposed mechanism is plausible.

2. Experimental

The TDIROF electrodes were prepared by thermal decomposition of a precursor solution (0.25 mol·L^{-1} H_2IrCl_6(99.9%, ABCR GmbH & Co, Karlsruhe, Germany) in i-propanol (99.8%, Merck KGaA, Darmstadt, Germany)) on a titanium substrate (grade 2, BIBUS METALS AG, Fehraltorf, Switzerland) as previously reported [7]. The titanium was sand blasted, treated in 1 mol·L^{-1}oxalic acid (99.5%, Fluka Chemie GmbH, Buchs, Switzerland) at 95 °C for one hour, rinsed with nanopure water and dried in an oven at 105 °C for 5 minutes. Several layers were deposited to reach the final loading. Each IrO_2 layer was applied by pipetting the precursor solution onto one side of the substrate and distributing it evenly with a brush. The i-propanol was evaporated in an oven at 105 °C for 10 minutes followed by a tempering of the electrodes at 500 °C for 10 minutes. A pair of rectangular electrodes (5 cm·4 cm) was loaded with 0.63 ± 0.00 mg·cm^{-2} and three RDEs (diameter 15 mm) with 0.81 ± 0.14 mg·cm^{-2}. As a final step, the TDIROF was annealed at 500 °C for 1 hour. The electrodes were characterized using a scanning electron microscope (SEM, Nova NanoSEM 230, FEI, Hillsboro, USA). Elemental analysis was performed with an energy dispersive X-ray (EDX) system (INCA 4.15, X MAX 80, Oxford, UK) attached to the microscope. Results are provided in the supplementary information in section A.

The CV experiments in stagnant electrolyte were performed in a one-compartment cell (50 mL) with a three electrode setup. The rectangular TDIROF working electrode was pressed against a hole in the bottom of the cell exposing a geometric surface area of 0.5 cm^2 to the electrolyte. The sealing between the electrode and the cell was made out of a silicon O-ring. The reference electrode ($Hg/Hg_2SO_4/K_2SO_4$ (MSE), Ref 601, Radiometer Analytical, Villeurbanne, France) was contained in a Luggin capillary filled with saturated K_2SO_4 (99%, Fluka). The tip of the Luggin capillary was placed 2 mm above the working electrode. A Pt-wire (geometric surface area: 1.26 cm^2) was used as the counter electrode. A potentiostat (PGU10V-1A-IMP-S, Ingenieurbüro Peter Schrems, Münster, Germany) controlled the working electrode potential. The working electrode potential and the current density were recorded with the EcmWin software (EcmWin V2.4, Ingenieurbüro Peter Schrems). The temperature and pH were measured continuously (SenTix 41 connected to pH 196, WTW, Weilheim, Germany) but no temperature control was installed.

The same potentiostat and pH meter were used in the CV experiments on a RDE but another one-compartment cell (200 mL) with three electrodes was used. The TDIROF-RDE was sealed in a Teflon cylinder exposing a geometric surface area of 0.95 cm^2. The cylinder was plugged on the rotator (Jaissle Rotator, Jaissle Elektronik, Waiblingen, Germany) and inserted into the electrolyte from the top. The reference electrode (MSE, HgE 11, Sensortechnik Meinsberg, Waldheim, Germany) was contained in a Luggin capillary filled with saturated K_2SO_4 (99%, Fluka). The angled tip of the capillary was placed 3 mm from the RDE. A Pt-foil (geometric surface area: 10.62 cm^2) was utilized as the counter electrode.

The electrolyte temperature was controlled at 25 ± 0.1 °C with a thermostat (Colora Messtechnik GmbH, Lorch, Germany). All experiments were performed in 0.5 mol·L^{-1} Na_2SO_4 (99%, Merck) + 0.125 mol·L^{-1} $(NH_4)_2SO_4$ (99.5%, Merck) dissolved in nanopure water. The pH value was adjusted by dosing NaOH (99%, Merck).

3. Calculations

We developed a dynamic numerical 1D-model to simulate pH, NH_3 and NH_4^+concentrations in the Nernstian diffusion layer of the working electrode. The Nernstian diffusion layer was divided into segments of uniform thickness in which the concentrations were assumed to be homogeneous. The heterogeneous electrochemical reactions of direct ammonia oxidation and oxygen evolution were assumed to affect only the lowest of these segments which we will call the reaction zone. Oxygen evolution was taken into account according to Eq. (6) and direct ammonia oxidation was assumed to lead exclusively to molecular nitrogen for reasons of simplicity:

$$NH_3 \rightarrow 0.5N_2 + 3H^+ + 3e^- \quad (7)$$

The surface specific reaction rate r_X (mmol·cm^{-2}·s^{-1}) of the compound X was estimated based on the measured current density j (mA·cm^{-2}) according to Faraday's law:

$$r_{NH_3} = -\frac{j_{NH_3}}{F \cdot n_{NH_3}} \quad (8)$$

$$r_{O_2} = -\frac{j_{O_2}}{F \cdot n_{O_2}} \quad (9)$$

$$r_{H^+} = n_{O_2} \cdot r_{O_2} - n_{NH_3} \cdot r_{NH_3} \quad (10)$$

where F = 96485 C·mol^{-1} is the Faraday constant, n_{O2} = 4 (−) and n_{NH3} = 3 (−) are the number of electrons transferred according to Eqs. (6) and (7).

The current density was allocated to the two electrochemical processes as follows:

$$j_{NH_3} = j_{NH} - j_b \; if: \; 0.3\,V < E_w < 0.68\,V \; and \; j_{NH_3} > 0\,mA \cdot cm^{-2} \quad (11)$$

$$j_{O_2} = j_{NH} - j_b \; if: \; 0.68\,V < E_w \; and \; j_{O_2} > 0\,mA \cdot cm^{-2} \quad (12)$$

The subscript *NH* denotes the current density measured during CV in 0.5 mol·L^{-1} Na_2SO_4 + 0.125 mol·L^{-1} $(NH_4)_2SO_4$ + NaOH and *b* denotes the background current density measured in 0.5 mol·L^{-1}Na_2SO_4 + NaOH. The j_b was subtracted to account for non-faradaic currents. E_w (V) is the potential of the working electrode.

The acid-base equilibrium of ammonia was modeled according to the mass action law in all segments individually and was assumed to be in equilibrium instantaneously. The conditional equilibrium constant (K_c) was calculated from $K = 10^{-pK_a}$ (pK_a = 9.25 [12]) with the activity coefficients of NH_3 ($\gamma_{NH_3} = 1$) and NH_4^+ ($\gamma_{NH_4} = 0.42$) accounting for the ionic strength I_c = 1.88 mol·L^{-1} in the supporting electrolyte.The activity coefficients were estimated in the chemical speciation software PHREEQC [13] using the Pitzer approach with a database extended by Pitzer parameters for ammonium [6]. The pK_c-value was found to be 9.62.

The concentration of X was denoted with c_X in mol·L^{-1}.

$$K_C = K \cdot \frac{\gamma_{NH_4}}{\gamma_{NH_3}} = \frac{c_{NH_3} \cdot c_{H^+}}{c_{NH_4^+}} \quad (13)$$

The mass flux $J_{Xi,i+1}$ (mmol·cm^{-2}·s^{-1}) of species X from segment i to segment $i+1$ was modeled with Fick's first law of diffusion (Eq. (14)). The mass flux by migration was neglected because of the high conductivity of the used electrolytes [14].

$$J_{Xi,i+1} = -D_X \frac{(c_{X,i} - c_{X,i+1})}{\Delta y} \quad (14)$$

The values of the implemented diffusion coefficients were D_{NH3} = 1.5·10^{-5} cm^2·s^{-1}, D_{NH4+} = 1.957·10^{-5} cm^2·s^{-1}, D_{H+} = 9.311·10^{-5} cm^2·s^{-1} [12] and Δy (cm) was the thickness of one segment in perpendicular direction to the electrode surface.

When an RDE was used, the thickness of the Nernstian diffusion layer δ_N (cm) was defined by the hydraulic conditions and could be calculated with Eq. (15) [15] depending on the angular velocity ω (s^{-1}), the kinematic viscosity of water ν = 8.93·10^{-3} cm^2·s^{-1} and the diffusion coefficient of ammonia.

$$\delta_N = 1.6 \cdot \omega^{-1/2} \cdot \nu^{1/6} \cdot {D_{NH_3}}^{1/3} \quad (15)$$

This numerical model was implemented in Berkeley Madonna (Berkeley Madonna Inc. Berkeley, USA, Version 8.3.18).

4. Results

4.1. CV experiments in stagnant and agitated electrolytes

The cyclic voltammograms in Fig. 1 show a strong inhibition of direct ammonia oxidation on our TDIROF electrodes in immediately consecutive scans confirming the findings of Kapałka *et al.* [7]. The ammonia oxidation peak in the forward scans (a1) as well as the ammonia oxidation peak in the backward scans (a2) decreased continuously from the first to the fifth scan. The peak a1 decreased

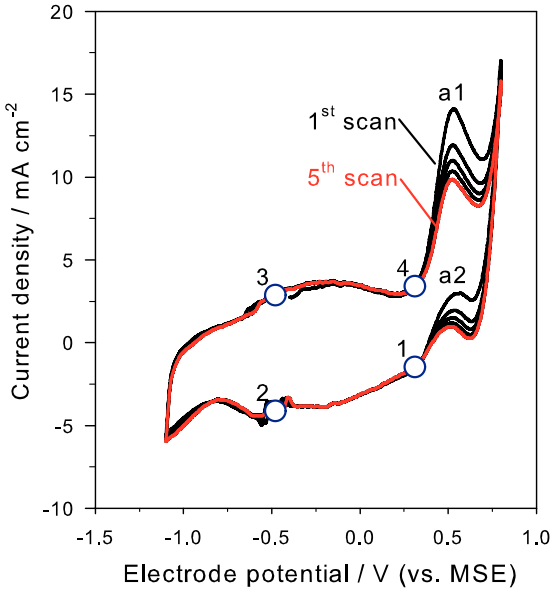

Fig. 1. Five consecutive scans on a TDIROF electrode in 0.5 mol·L^{-1} Na_2SO_4 + 0.125 mol·L^{-1} $(NH_4)_2SO_4$ + NaOH at pH = 9.25. Scan rate 200 mV·s^{-1}, upper return potential: 0.8 V vs. MSE, lower return potential: -1.1 V vs. MSE, T = 25.2 °C, counter electrode: Pt-wire. The circles (○) at 0.3 and -0.5 V vs. MSE mark the points at which the concentration profiles in Fig. 5 and Fig. 7 were calculated.

in five scans by 32%. It is important to note that the scans were performed without interruption; the lag phase was 19 seconds between two consecutive ammonia oxidation peaks. Thus, the time for diffusion to equilibrate the reactant and pH gradients in the Nernstian diffusion layer was limited.

In compliance with the interpretation of Kapałka *et al.* [7], the peak a2 appears because ammonia is not oxidized in the OER. It was hypothesized that NH_3 oxidation requires the redox couple $IrO(OH)_2/IrO_2(OH)$ present at anode potentials of about 0.3 to 0.7 V vs. MSE. Above potentials of 0.7 V vs. MSE, the iridium is completely oxidized to IrO_3 which excludes the oxidation of ammonia in the OER. However, the oxidation to IrO_3 is reversible and therefore ammonia oxidation restarts in the backward scan.

The lower return potential was clearly above the HER in which protons would be consumed according to Eq. (16).

$$2H^+ + 2e^- \rightarrow H_2 \quad (16)$$

As the HER was not reached, the protons released during the anodic reactions of ammonia oxidation (Eq. (2)–(4)) or oxygen evolution (Eq. (6)) were not consumed by hydrogen evolution during the cathodic polarization of the electrode. This means that the reduction of the peaks a1 and a2 could very well result from a reactant limitation due to a drop in local pH.

Fig. 2A shows five immediately consecutive CV scans in which the TDIROF electrode was polarized moderately into the HER (lower return potential -1.5 V vs. MSE). The ammonia oxidation peaks a1 and a2 were nearly identical, just the first scan showed slightly smaller peaks. An even more pronounced difference between the first and the consecutive scans can be seen in Fig. 2B presenting the data of an experiment where the electrode was strongly polarized into the HER (lower return potential -1.7 V vs. MSE). In this case, the ammonia oxidation peaks of the scans two to five (again all nearly identical) were clearly higher than in the first scan.

In contrast to the experiment where the HER was not reached (Fig. 1), the polarization of the working electrode into the HER resulted in the consumption of protons according to Eq. (16). The longer the electrode was polarized into the HER, the higher were the ammonia oxidation peaks a1 and a2 in the following anodic

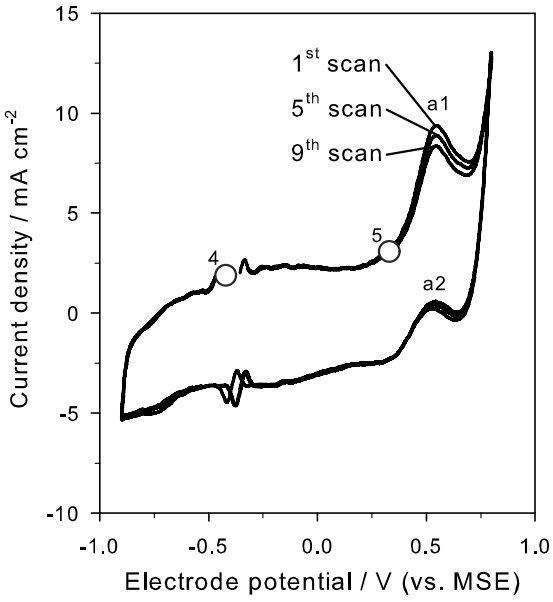

Fig. 3. Three CV scans on TDIROF in 0.5 mol·L^{-1} Na_2SO_4 + 0.125 mol·L^{-1} $(NH_4)_2SO_4$ + NaOH at pH = 9.25. An idle period of 4 minutes was introduced between each scan during which the electrolyte was stirred. The points (4) at -0.4 V and (5) at 0.3 V vs. MSE at which the concentration profiles in Fig. 6 were calculated are indicated with the circles (○). Scan rate 200 mV·s^{-1}, upper return potential: 0.8 V vs. MSE, lower return potential: -0.9 V vs. MSE, T = 23.4 °C, counter electrode: Pt-wire.

polarizations. This very likely resulted from a higher NH_3 concentration in the reaction zone after strong hydrogen evolution.

Compared to the experiment with immediate consecutive scans (Fig. 1), a considerably lower reduction of a1 and a2 was observed if an idle period of 4 minutes was inserted between individual scans, even if the lower return potential was kept above the HER (Fig. 3). The peak a1 decreased by no more than 11% from the first to the ninth scan which is clearly less than with immediately consecutive scans. This finding corroborates our hypothesis of an effect in the diffusion layer. Due to the diffusion of protons, ammonia and

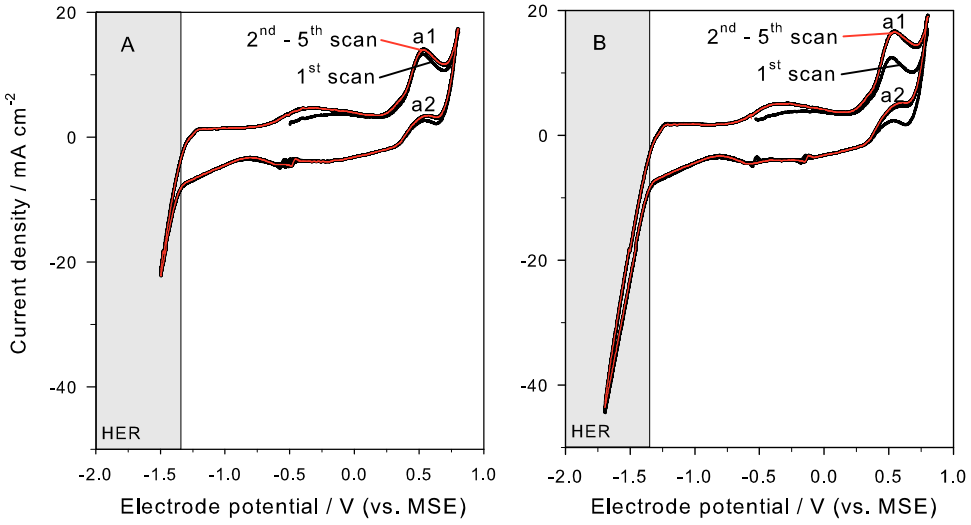

Fig. 2. A: Five consecutive scans on TDIROF in 0.5 mol·L^{-1} Na_2SO_4 + 0.125 mol·L^{-1} $(NH_4)_2SO_4$ + NaOH with a lower return potential of -1.5 V vs. MSE. B: The same as in A but with a lower return potential of -1.7 V vs. MSE. The red solid line marks the 5th scan. Scan rate 200 mV·s^{-1}, upper return potential: 0.8 V vs. MSE, pH = 9.25, T = 25.3 °C, counter electrode: Pt-wire.

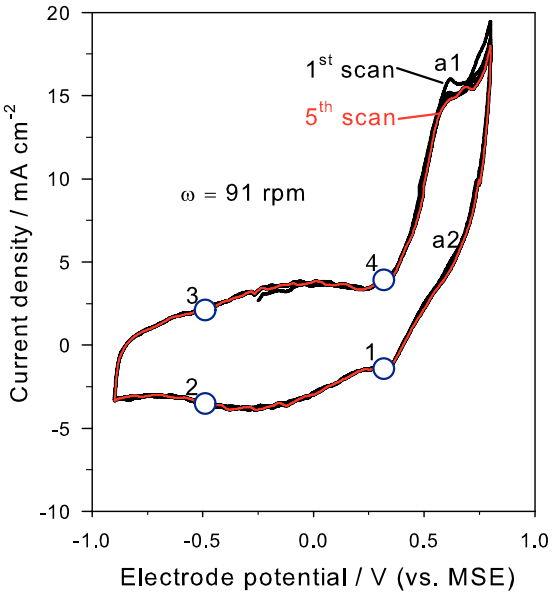

Fig. 4. Five consecutive scans on a rotating TDIROF electrode in 0.5 mol·L^{-1} Na_2SO_4 + 0.125 mol·L^{-1} $(NH_4)_2SO_4$ + NaOH at pH = 9.25. The circles (○) at 0.3 and -0.5 V vs. MSE mark the points at which the concentration profiles in Fig. 7 were calculated. Scan rate 200 mV·s^{-1}, upper return potential: 0.8 V vs. MSE, lower return potential: -0.9 V vs. MSE, T = 25.0 °C, counter electrode: Pt-foil.

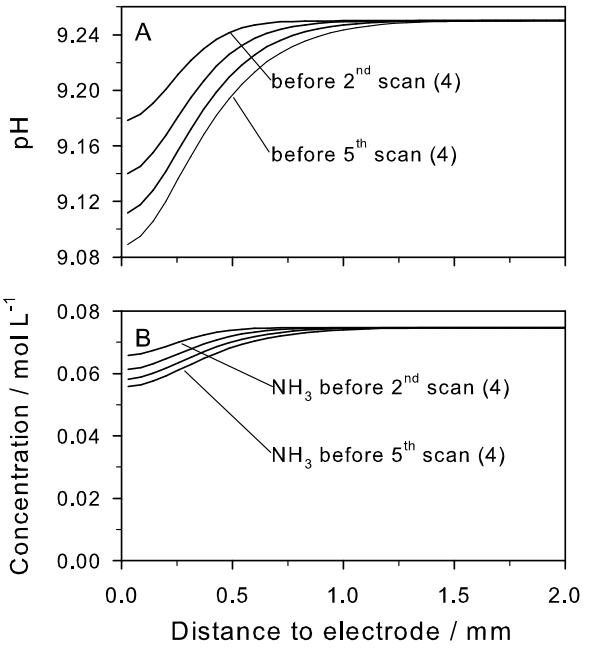

Fig. 5. A: Calculated pH profiles in the vicinity of the electrode. B: NH_3 concentration profiles in the vicinity of the electrode. The profiles correspond to point (4) just before the ammonia oxidation peaks a1 appeared in the experiment presented in Fig. 1 (immediately consecutive scans, bulk pH = 9.25).

ammonium, similar NH_3 concentrations must have been reached in the reaction zone prior to each anodic polarization which resulted in comparable ammonia oxidation peaks.

If the much lower decrease of a1 and a2 would have resulted from the reduction of poisonous N_{ads}, a reduction peak would have been expected in the backward scans. However, this was neither the case with or without idle periods between the scans (Fig. 1 and Fig. 3, respectively). Also the reduction of N_{ads} during the idle phase was very unlikely because the OCP was almost constant between the scans (mean OCP value of all idle periods -0.413 ± 0.003 V vs. MSE) and certainly did not reach values below the lower return potential (supplementary information B).

In Fig. 4 we present five immediately consecutive cyclic voltammograms recorded on an RDE at an angular velocity of 91 rpm. In contrast to the scans in stagnant electrolyte without idle phase, the scans following the first scan on the RDE did not result in a strong decrease of the direct ammonia oxidation peaks a1 or a2. In fact, the peak a1 only decreased by 5% from the first to the second scan. In the following scans, the decrease of peak a1 was small (around 0.6% in each scan) resulting in a total peak decrease from the first to the fifth scan of 7%.

Also in this experiment, the lower return potential (-0.9 V vs. MSE) was chosen clearly above the HER and even 0.2 V higher than in the experiment in stagnant electrolyte (Fig. 1). The time in which concentration gradients could even out was short (17 s) and the protons released during direct ammonia oxidation (Eq. (1)–(4)) and oxygen evolution (Eq. (6)) could not be consumed by hydrogen evolution. However, by making use of an RDE we were able to control the hydraulics at the working electrode and therewith to reduce δ_N. The consequences of this can be shown with our model calculations and are presented in the next section.

4.2. Concentration profiles in the Nernstian diffusion layer during CV

The electrochemical measurements all supported our hypothesis but they did not show how the diffusion in the electrolyte proceeded and whether the proposed mechanism would be plausible on the observed special and temporal scale. To get more information about the concentration profiles in the diffusion layer we used the dynamic computer model. The initial conditions of the three state variables were chosen as $c_{NH_3} = 0.07476$ *and* $c_{NH_4^+} = 0.1752$ molN·L^{-1} and pH = 9.25 in all simulations.

In Fig. 5, simulated concentration profiles are given for the characteristic points of the voltammogram in Fig. 1. The concentration profiles show that the time between ammonia

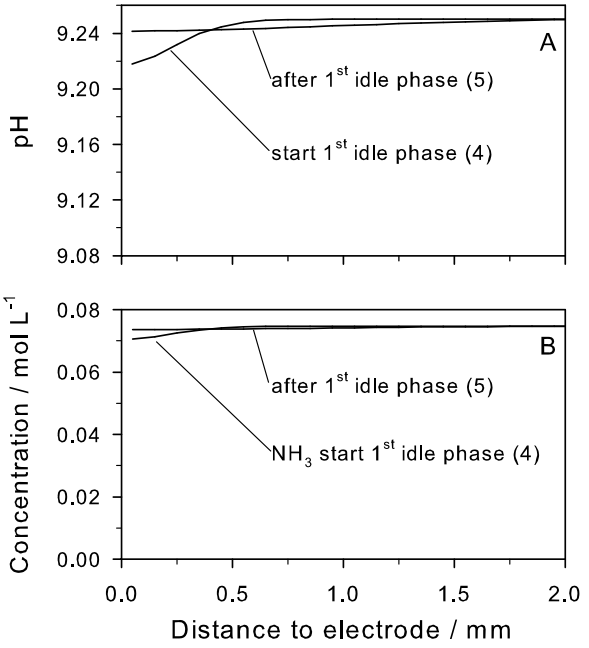

Fig. 6. A: Calculated pH profiles. B: NH_3 concentration profiles. The profiles correspond to the points (4) and (5) in the first idle phase indicated in Fig. 3 (4 minutes idle phase between scans, bulk pH = 9.25).

oxidation peaks in immediately subsequent scans was too short for the pH gradient to equalize (Fig. 5A). Consequently, the regions in the vicinity of the electrode became more and more acidic with every scan. Due to the acid-base equilibrium, the change in pH resulted in a strong shift of ammonia speciation. Namely, the NH_3 concentration dropped considerably (Fig. 5B). Thus, the concentration of the reactant (NH_3) became lower during every anodic scan resulting in smaller direct ammonia oxidation peaks.

Figs. 6A and B display simulated concentration profiles at the points marked in Fig. 3 during the experiment where an idle phase of 4 minutes was inserted between the scans. The profiles at the beginning of the first idle phase were calculated at the same point in time since the start of the experiment as the profiles calculated before the second scan in the experiment without an idle phase. These concentration profiles form Fig. 5 and Fig. 6 are directly comparable. The profiles in Figs. 6A and B were less pronounced because the anodic currents in the foregoing scan were smaller. After the first idle phase, just before the second anodic polarization started (point (5) in Fig. 3), there still was a small shift of ammonia speciation in the reaction zone (Fig. 6B). This explains the small reduction of the ammonia oxidation peaks in the following scan and in all additional cycles until the ninth scan. The idle time between the scans allowed concentrations to equalize almost completely before a new anodic polarization so that comparable ammonia oxidation peaks were measured.

In stagnant electrolyte, the Nernstian diffusion layer has no limit and could theoretically expand deep into the bulk liquid. From the concentration profiles in Fig. 5A it can be deduced that the maximal δ_N was close to 1.5 mm during the experiment presented in Fig. 1. On the RDE, δ_N was hydraulically controlled and much thinner. With Eq. (15) it was calculated to be $\delta_N = 0.15$ mm for the applied rotational speed of 91 rpm. The consequences were the buildup of distinctly different concentration profiles of H^+, NH_4^+ and NH_3 compared to the stagnant electrolyte leading to a considerably different diffusion behavior.

A comparison of four concentration profiles between the first anodic polarization and the second anodic polarization in stagnant electrolyte (A, B, and C) and in agitated electrolyte (D, E, and F) is shown in Fig. 7. In the stagnant electrolyte and on the RDE, a speciation shift due to a change in local pH appeared. However, when δ_N was hydraulically controlled on the RDE the concentration gradients evened out much faster. The reason for this was the more pronounced concentration gradients due to a thinner and limited Nernstian diffusion layer. The result was faster diffusion allowing concentrations to draw level quickly. Consequently, the concentration of NH_3 in the reaction zone at point 4 prior to the second anodic polarization was much closer to the one found prior to the first scan (compare the profiles 4 at distance 0 from the electrode in Figs. 7B and E). This is remarkable and demonstrates the importance of δ_N. It should be noted that the time until point 4 was reached in the CV on the RDE was shorter, because the lower return potential was higher than in the experiments with stagnant electrolyte (Fig. 1).

5. Discussion

5.1. Mechanisms inhibiting direct ammonia oxidation

Gerischer and Mauerer [9] distinguished between a fast and a slow passivation of direct ammonia oxidation on Pt. They found that the fast passivation was reversible by simply letting the working electrode rest at OCP. On the other hand, the slow

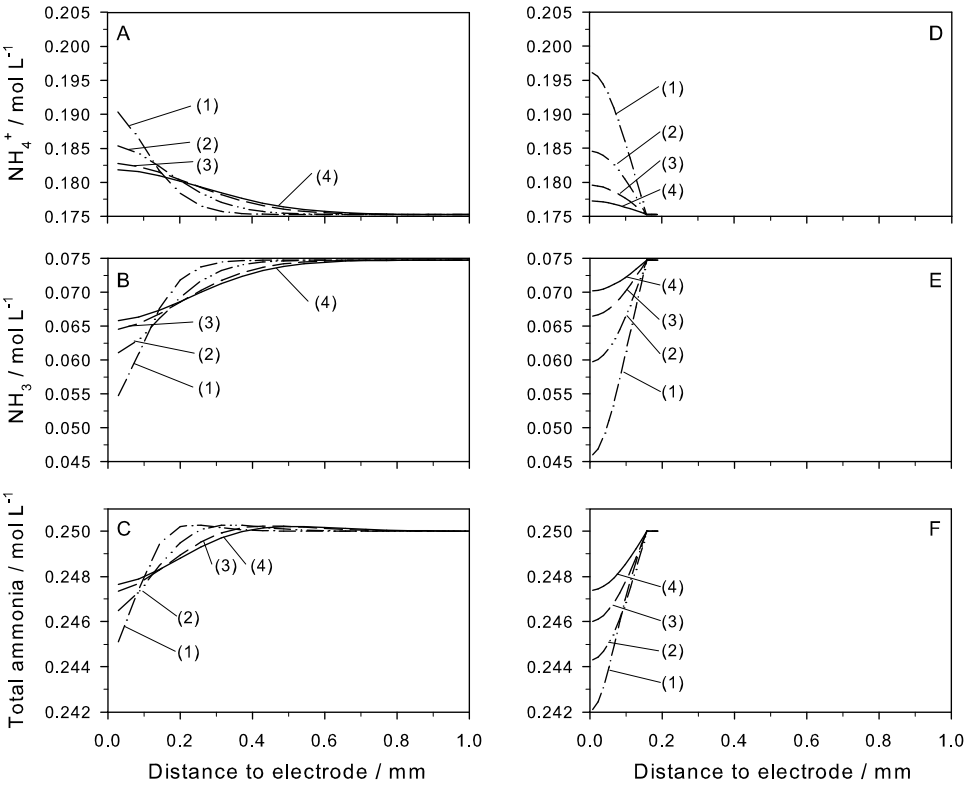

Fig. 7. A, B, and C: Calculated concentration profiles during the second scan of the experiment in stagnant electrolyte presented in Fig. 1. D, E, and F: Calculated concentration profiles during the second scan of the experiment on the RDE presented in Fig. 4 during which the Nernstian diffusion layer was hydraulically controlled at $\delta_N = 0.15$ mm. The numbers in the plots correspond to the numbers in the Fig. 1 and Fig. 4 indicating the point in time at which the profile was calculated.

passivation was found to be irreversible and was attributed to surface poisoning by N_{ads}. This also meant that the fast passivation could not result from surface poisoning by N_{ads} because the fast passivation was reversible.

Analogous to the platinum case, we argue that the fast inhibition of direct ammonia oxidation on TDIROF, as observed by Kapałka *et al.* [7] and in our experiments (Fig. 1), cannot result from surface poisoning by N_{ads}. The experiment presented in Fig. 2 showed that it was enough to let the TDIROF electrode rest at OCP during an idle phase of 4 minutes to restore the catalytic activity of the electrode. Thus, the fast inhibition on TDIROF was reversible. Gerischer and Mauerer [9] showed that N_{ads} can only be removed from Pt at high temperatures due to the high binding energy of N_{ads}. De Vooys *et al.* [11] estimated the binding energy of N_{ads} on Pt to be 394 $kJ \cdot mol^{-1}$ and Wang *et al.* [16] calculated a value of 373 $kJ \cdot mol^{-1}$ on oxygen rich IrO_2. These binding energies are in the same order of magnitude. Therefore, the passivation of IrO_2 by N_{ads} should be irreversible too but it was not. Furthermore, if surface poisoning by N_{ads} would be the relevant mechanism, decreasing ammonia oxidation peaks would also be expected to appear on the RDE (Fig. 4) but they did not. For these reasons, the fast inhibition of direct ammonia oxidation cannot result from surface poisoning by N_{ads}. However, our results do not reveal whether surface poisoning by N_{ads} could appear during long term anodic polarization.

The formation of surface oxides can also be ruled out as the reason for the fast inhibition of direct ammonia oxidation in subsequent CV scans. In the study by Kapałka *et al.* [7] it was argued that direct ammonia oxidation involves the surface redox couple $IrO(OH)_2/IrO_2(OH)$. The complete oxidation of $IrO_2(OH)$ to IrO_3 in the OER was therefore assumed to stop direct ammonia oxidation. However, the appearance of the peak a2, again resulting from ammonia oxidation on $IrO(OH)_2/IrO_2(OH)$, indicated that IrO_3 was reduced at electrode potentials higher than 0.6 V vs. MSE. Thus, the passivation by IrO_3 was cleared away in the backward scans and the subsequent forward scan was not affected. Additionally, a passivation of the TDIROF surface by IrO_3 should have resulted in the same peak decrease in stagnant electrolyte (Fig. 1) as on the RDE (Fig. 4) but this was not the case.

Our experiments and the simulations of the processes in the Nernstian diffusion layer provided convincing evidence that direct ammonia oxidation can be strongly inhibited by a reactant limitation induced by a local pH drop in the vicinity of the electrode. This mechanism was already put forward by Kapałka *et al.* [7] to explain their observation that deeper polarization of the electrode into the OER resulted in a reduced ammonia oxidation peak a2 due to the release of protons during oxygen evolution and it was mentioned in a recent work on ammonia oxidation kinetics [17]. The mechanism can also explain why the direct ammonia oxidation peaks increased when we strongly polarized the electrode into HER. The consumption of protons changed the local pH towards more positive values making more reactive NH_3 available in the subsequent forward scans. This resulted in higher peaks a1 and a2. Finally, our simulations showed that the proposed mechanism is reasonable on the observed spatial and temporal scale.

5.2. Modeling the Nernstian diffusion layer

The model shows the relative importance of the processes occurring in the reaction zone due to direct ammonia oxidation and oxygen evolution: the consequence of the NH_3 removal was that the total ammonia dropped close to the electrode (Fig. 7C). However, the more important process leading to NH_3 limitation was the pH drop and the shift in ammonia speciation. A comparison of the profiles (1) in Figs. 7B and C shows that the NH_3 concentration dropped by about 20 $mmol \cdot L^{-1}$ while the concentration of total ammonia only declined by 5 $mmol \cdot L^{-1}$. This led to concentration gradients of NH_3 but also of NH_4^+. It is interesting to note that the gradient of NH_3 was more pronounced than the one of NH_4^+ which resulted from the lower concentration of total ammonia towards the electrodes.

Fig. 7C shows another interesting detail. The concentration of total ammonia went through a maximum higher than the value in the bulk liquid in all four profiles. This maximum moved towards the bulk electrolyte and formed a total ammonia wave propagating away from the electrode. The origin of this wave was the difference in the diffusion coefficients of NH_3 and NH_4^+. Even though the concentration gradient for NH_3 was more pronounced than the one of NH_4^+ the higher diffusion coefficient of NH_4^+ led to a stronger diffusion of that compound resulting in a higher ammonia mass flow away from the electrode in those regions that were not yet affected by ammonia depletion. Therefore, the shift in ammonia speciation not only resulted in a strong reactant limitation in the reaction zone but also in a transport of total ammonia away from the reaction zone.

5.3. Overcoming the inhibition mechanism

It should be feasible to use TDIROF for continuous ammonia oxidation in aqueous solutions, if the reactant limitation due to the proposed inhibition mechanism can be overcome. The reactant limitation may be resolved in three ways. The first possibility is to work at highly alkaline conditions although this bears the risk of ammonia volatilization and may requires the dosage of a base. In these situations the excess of hydroxyl ions ensures sufficient alkalinity to prevent a pH drop. Such high pH conditions were applied in some laboratory studies showing continuous ammonia oxidation on other electrode materials. The group of Botte used Pt, Pt-Ir and Pt-Ir-Rh electro-catalysts [17–19] and made sure to have an excess of KOH present in the electrolyte. The same principle was applied in a study by Le Vot *et al.* [20] using Pt in which a surplus of NaOH was ensured.

A drop in local pH can also be avoided by buffering the electrolyte. A naturally occurring buffer system in the suitable pH range is the carbonate/bicarbonate buffer system ($pK_a = 10.33$ [12]). However, it was shown that carbonate oxidation competes with direct ammonia oxidation on TDIROF which led to negligible ammonia oxidation at high pH values [21]. On the other hand, very high carbonate to ammonia ratios did not influence direct ammonia oxidation on the graphite electrode [5]. The small ammonia removal rates in that study probably resulted from low ammonia concentrations (<400 $mgN \cdot L^{-1}$) and pH values (<9) in combination with non-optimized hydraulic conditions.

A third option was demonstrated with our RDE experiments and consists of reducing δ_N by controlling the hydraulic conditions at the electrode. The group of Eil-Hee Lee published several studies on the oxidation of ammonia in stacked electrolysis cells in which non-buffered electrolytes without chloride were recirculated [22–24]. The induced convection at the electrodes probably reduced δ_N resulting in continuous direct ammonia oxidation. The very high removal rates (3000 $gN \cdot m^{-2} \cdot d^{-1}$, [22]) may be explained with the high ammonia concentration (1 $mol \cdot L^{-1}$) at elevated pH values (pH = 12) and the considerable current densities that were applied (80 $mA \cdot cm^{-2}$). Process inhibition did not seem to be an issue. The ammonia oxidation rates were stable in an undivided cell during 1.5 hours of electrolysis.

5.4. Implications of the pH effect for electrolytic processes

The proposed inhibition mechanism is primarily important for ammonia oxidation in weakly buffered and moderately alkaline

aqueous solutions and therefore of outstanding importance for wastewater treatment. In such applications, it appears to be most promising to improve the hydraulic conditions in the electrolysis cells because neither working under highly alkaline conditions nor strong buffering of the wastewater are reasonable options because chemicals would need to be added.

For other important applications of direct ammonia oxidation such as the use in alkaline fuel cells or the production of high-purity hydrogen the pH effect can be avoided by working at strongly alkaline conditions or in non-aqueous media. It has been shown by Peng *et al.* [25] that direct ammonia oxidation in saturated acetonitrile was not affected by any form of process inhibition on Pt and Pd electrodes. This indicates that in non-aqueous solutions a similar pH effect as in aqueous solutions must not necessarily exist.

However, similar pH effects as the one observed in the current study for direct ammonia oxidation might also play an important role for other electrochemical reactions that are sensitive to pH. For instance, an early study by Landolt and Ibl [26] pointed out that the pH in the Nernstian diffusion layer influenced chlorate formation in concentrated NaCl solutions. Similar to the ammonia case, the protons released during hypochlorite oxidation itself (Eq. (17)) and oxygen evolution (Eq. (6)) were argued to result in lower amounts of the more reactive hypochlorite ion according to the acid-base equilibrium in Eq. (18) leading to slower chlorate formation.

$$6OCl^- + 3H_2O \rightarrow 2ClO_3^- + 4Cl^- + 6H^+ + 1.5O_2 + 6e^- \quad (17)$$

$$ClO^- + H^+ \rightleftharpoons HClO \quad (18)$$

6. Conclusions

Fast inhibition of direct ammonia oxidation on TDIROF electrodes is caused by a local pH drop in the Nernstian diffusion layer. The pH drop results from anodic processes such as oxygen evolution and direct ammonia oxidation itself. Thus, direct ammonia oxidation is partially self-inhibited. This pH effect can easily be mistaken for surface poisoning by N_{ads} because both effects are related to direct ammonia oxidation.

Since surface poisoning was found to play a minor role on short timescales, continuous ammonia removal by direct oxidation must be possible if optimal hydraulic conditions prevail in the electrolysis cell. Direct ammonia oxidation would be advantageous, because lower anode potentials can be applied resulting in a higher current efficiency and a lower energy demand. Additionally, the formation of chlorinated by-products can be prevented. Nevertheless, surface poisoning may be an issue in long term operation of TDIROF anodes leading to slow process deactivation.

The inhibition mechanism we found is generally valid and not related to a specific type of electrode. Therefore, the challenge for successful application of direct ammonia oxidation for the treatment of wastewater is to overcome the local pH decrease. This could be achieved by reducing the Nernstian diffusion layer to a minimum.

Acknowledgments

We thank Karin Rottermann and Claudia Bänninger-Werffeli for the chemical analysis and we acknowledge the support from the Electron Microscopy Center at Empa (Swiss Federal Institute for Materials Science and Technology, Duebendorf, Switzerland). Cristina Fritzsche is acknowledged for her experiments initiating this research. We thank Christos Comninellis at the Swiss Federal Institute of Technology in Lausanne (EPFL) for inspiring discussions. Furthermore, we thank the Bill and Melinda Gates Foundation for financing this study as part of the VUNA project (www.vuna.ch, Grant No. OPP1011603).

References

[1] M. Muthuvel, G.G. Botte, Trends in Ammonia Electrolysis, in: R.E. White (Ed.), Modern Aspects of Electrochemistry, vol. 45, Springer New York, New York, 2009, pp. 207–245 No. 45.
[2] N.J. Bunce, D. Bejan, Mechanism of electrochemical oxidation of ammonia, Electrochimica Acta 56 (2011) 8085–8093.
[3] R. Lan, S.W. Tao, Direct Ammonia Alkaline Anion-Exchange Membrane Fuel Cells, Electrochem. Solid State Lett. 13 (2010) B83–B86.
[4] F. Vitse, M. Cooper, G.G. Botte, On the use of ammonia electrolysis for hydrogen production, J. Power Sources 142 (2005) 18–26.
[5] H. Zöllig, C. Fritzsche, E. Morgenroth, K.M. Udert, Direct electrochemical oxidation of ammonia on graphite as a treatment option for stored source-separated urine, Water Research 69 (2015) 284–294.
[6] A. Kapałka, A. Cally, S. Neodo, C. Comninellis, M. Wächter, K.M. Udert, Electrochemical behavior of ammonia at Ni/Ni(OH)2 electrode, Electrochemistry Communications 12 (2010) 18–21.
[7] A. Kapałka, S. Fierro, Z. Frontistis, A. Katsaounis, S. Neodo, O. Frey, N. de Rooij, K. M. Udert, C. Comninellis, Electrochemical oxidation of ammonia (NH4+/NH3) on thermally and electrochemically prepared IrO2 electrodes, Electrochimica Acta 56 (2011) 1361–1365.
[8] A. Kapałka, L. Joss, A. Anglada, C. Comninellis, K.M. Udert, Direct and mediated electrochemical oxidation of ammonia on boron-doped diamond electrode, Electrochemistry Communications 12 (2010) 1714–1717.
[9] H. Gerischer, A. Mauerer, Studies on anodic oxidation of ammonium on platinum electrodes, Journal of Electroanalytical Chemistry 25 (1970) 421–433.
[10] C. Zhong, W.B. Hu, Y.F. Cheng, Recent advances in electrocatalysts for electro-oxidation of ammonia, J. Mater. Chem. A 1 (2013) 3216–3238.
[11] A.C.A. de Vooys, M.T.M. Koper, R.A. van Santen, J.A.R. van Veen, The role of adsorbates in the electrochemical oxidation of ammonia on noble and transition metal electrodes, Journal of Electroanalytical Chemistry 506 (2001) 127–137.
[12] W.M. Haynes (Ed.), CRC Handbook of Chemistry and Physics, 95th Edition (Internet Version 2015), CRC Press/Taylor and Francis, Boca Raton, FL.
[13] D.L. Parkhurst, C.A.J., Appelo, User's guide to PHREEQC (version 2): A computer program for speciation, batch-reaction, one-dimensional transport, and inverse geochemical calculations, USGS Water-resources investigations report; 99-4259, U.S.G. Survey, Denver CO, USA, 1999.
[14] C.H. Hamann, W. Vielstich, Electrochemistry, WILEY-VCH Verlag GmbH & Co. KGaA, Weinheim, 2007.
[15] A.J. Bard, L.R. Faulkner, Electrochemical Methods: Fundamentals and Applications, John Wiley & Sons, New York, 2001.
[16] C.C. Wang, S.S. Siao, J.C. Jiang, Density Functional Theory Study of NHx (x = 0-3) and N-2 Adsorption on IrO2(110) Surfaces, J. Phys. Chem. C 114 (2010) 18588–18593.
[17] L.A. Diaz, A. Valenzuela-Muñiz, M. Muthuvel, G.G. Botte, Analysis of ammonia electro-oxidation kinetics using a rotating disk electrode, Electrochimica Acta 89 (2013) 413–421.
[18] B.K. Boggs, G.G. Botte, On-board hydrogen storage and production: An application of ammonia electrolysis, J. Power Sources 192 (2009) 573–581.
[19] E.P. Bonnin, E.J. Biddinger, G.G. Botte, Effect of catalyst on electrolysis of ammonia effluents, J. Power Sources 182 (2008) 284–290.
[20] S. Le Vot, D. Reyter, L. Roué, D. Bélanger, Electrochemical Oxidation of NH3 on Platinum Electrodeposited onto Graphite Electrode, Journal of the Electrochemical Society 159 (2012) F91–F96.
[21] V. Amstutz, A. Katsaounis, A. Kapałka, C. Comninellis, K.M. Udert, Effects of carbonate on the electrolytic removal of ammonia and urea from urine with thermally prepared IrO2 electrodes, J. Appl. Electrochem. 42 (2012) 787–795.
[22] K.W. Kim, Y.J. Kim, I.T. Kim, G.I. Park, E.H. Lee, Electrochemical conversion characteristics of ammonia to nitrogen, Water Research 40 (2006) 1431–1441.
[23] K.W. Kim, I.T. Kim, G.I. Park, E.H. Lee, Electrolytic decomposition of ammonia to nitrogen in a multi-cell-stacked electrolyzer with a self-pH-adjustment function, J. Appl. Electrochem. 36 (2006) 1415–1426.
[24] K.W. Kim, Y.J. Kim, I.T. Kim, G.I. Park, E.H. Lee, The electrolytic decomposition mechanism of ammonia to nitrogen at an IrO2 anode, Electrochimica Acta 50 (2005) 4356–4364.
[25] W. Peng, L. Xiao, B. Huang, L. Zhuang, J. Lu, Inhibition effect of surface oxygenated species on ammonia oxidation reaction, J. Phys. Chem. C 115 (2011) 23050–23056.
[26] D. Landolt, N. Ibl, On mechanism of anodic chlorate formation in concentrated NaCl solutions, Electrochimica Acta 15 (1970) 1165–1183.